Tribology in Industry

RESEARCH

Surface Saturation with Carbon Using Plasma Arc and Graphite Coating

V.H. Vu[a], A.E. Balanovskiy[b],*, V.T. Doan[a], V.T. Nguyen[a]

[a]*Vietnam-Russia Tropical Centre, Nha Trang, Vietnam,*
[b]*Engineering Technologies and Materials Department of National Research Irkutsk State Technical University, Irkutsk, Russia*

* Corresponding author:

A.E. Balanovskiy (iD)
E-mail: *fuco.64@mail.ru*

A B S T R A C T

This study presents the development of a novel equipment for carburizing, by means of a plasma arc and a graphite paste based on liquid glass. After processing by this method, the microstructure and microhardness of the hardened layer were studied. The assay revealed that during a brief plasma exposure, the surface layer was saturated with carbon to a concentration level, which corresponds to white cast iron. The microstructures and characteristics of the metal surface post plasma cementation were also studied. The main parameters of the cemented layer were determined: the depth of the cemented layer was 150-200 μm, microhardness was up to 1000 $HV_{0.2}$.

© 2021 Published by Faculty of Engineering

1. INTRODUCTION

The use of surface saturation with carbon to increase the hardness and wear resistance of steel has been known for a long time. In the XI century, people already knew how to turn mild malleable steel into hardenable solid steel by heating it in a powder, which was made from charcoal, bones, horns and other additives [1]. Over time, the technology of carburizing machine parts and tools has been improved and widely adopted due to its effectiveness. An important technological parameter of cementation technology that requires to improvement is the process duration.

Over the recent years, developments in scientific and technological progress enabled the use of concentrated heat sources (e.g. lasers, plasma, or electron beams) to harden the surface of metals and alloys [2,3]. When using these types of energy sources (heating), it becomes possible to obtain unique structures and properties of the surface layer that were previously unattainable. This is due to the fact that the use of concentrated heating sources makes it possible to heat the surfaces of parts with speeds several orders of magnitude higher than the heating rates of traditional heating methods. Because of

the surface layer's high heating and cooling rates, the mechanical properties and other important characteristics of materials are improved [4]. Highly concentrated heat sources (e.g. the plasma arc and jet), are also used to saturate the surface with carbon, nitrogen, and other elements, but this area of research has not been adequately studied. Nevertheless, they exhibit some advantages compared to traditional methods: high performance, lack of restrictions on the configuration of parts, and the absence of mechanical deformation [5].

Recent works [6,7] have shown the prospect of carburizing steel surfaces using a plasma arc. In these works, pastes that consist of graphite, liquid glass, water, and oil-coolant, were considered for the carburizing process. This enables the saturation of metal surfaces with carbon either with or without surface melting. Works devoted to the description of cemented layer structures post plasma carburization, have so far produced insignificant results, when compared to laser and electron-beam treatment.

It is known that in the 1940s and 1950s the USSR performed studies on the use of a welding arc and a graphite electrode to harden the surface of steel [8]. The arc oscillation was performed using an alternating magnetic field so as to avoid surface melting. However, this technology was not implemented in industry due to the accumulation of heat in the electrode. Meanwhile, in the USA, a continuous supply of additional metal (wire) to the arc was proposed to automate the argon-arc welding process. The new arc was initially called "compressed", but subsequently became known as "plasma". If the arc burns between the electrode and the workpiece, it is called a "direct arc" or a "plasma arc", but if it burns between the electrode and the nozzle, it is referred to an "indirect arc" or "plasma jet". The plasma jet was primarily used for sputtering and the plasma direct arc was used for welding and cutting [9,10]. In the 1980s, XX century plasma devices began to be widely used in industry for welding, cutting, spraying and hardening of parts such as mining equipment and automobile camshafts [8].

Gas tungsten arc welding equipment, less complicated and more common, also produces a plasma arc. But the use of these apparatuses for surface treatment (hardening, carburizing) is limited. The problem is that the plasma arc obtained by such an apparatus has a small heating spot, therefore the width of the hardened track is negligible. To solve this problem, an oscillation of the arc by a magnetic field was used [5,11]; as a result, the track width was expanded to 15–20 mm. However, it should be noted that, the arc generated by this type of equipment (direct arc) has a greater sensitivity to setting the mode. The process easily deviates from the optimum mode during manual hardening, and surface fusion or disappearance of the hardened layer is caused.

Therefore, the development of automation technology of this type is an important aspect for plasma surface treatment. In this work, we developed an equipment for automating the local surface carburizing (hardening) process using a graphite paste and the electric (plasma) arc used in TIG welding.

2. EXPERIMENT

2.1 Equipment for surface carburizing

The equipment for surface carburizing consists of: a personal computer (1), a TIG 250P device (2), a frame (3), with a mechanism for supporting the movement of tables, a welding torch (4), the table (5) for fixing flat workpiece, the table (6) is equipped with a jaw chuck K80 (7) for holding and rotating the cylindrical sample (Fig. 1). Equipment parameters are given in table 1.

Table 1. Installation options.

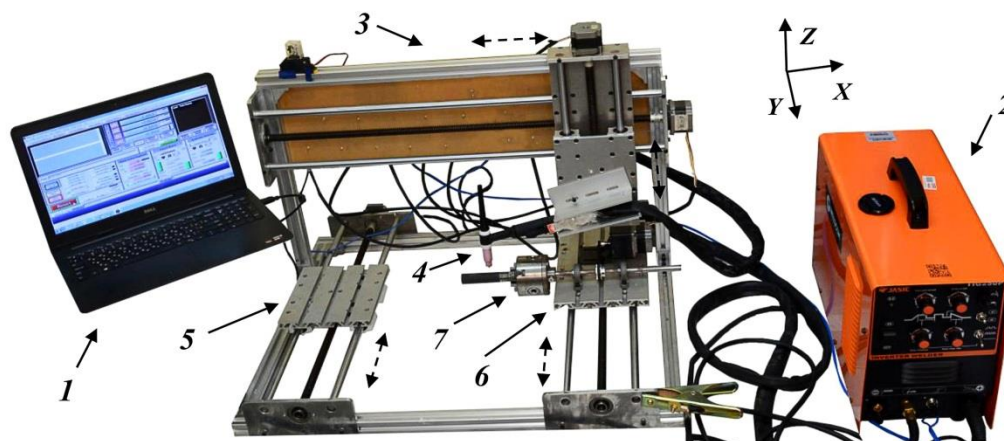|	
X Y Z working area (mm)	750x550x300
Table Dimensions (mm)	200x200; 200x300
Outside size (mm)	800x600x600
Frame structure	V slot aluminum profile
X, Y, Z structure	Ball screw
Software	Mach3
A structure	Toothed belt drive
Driving system:	Stepper driver and motor
Voltage:	220V/50HZ
Operating system	Windows XP/7 (32)

Fig. 1. Equipment for surface saturation.

The PC (1) is used to provide the command signals to the machine, and is crucial for the uninterrupted operation of the equipment. The PC (1) is pre-installed with the Mach 3 software, which turns it into an industrial machine control station. Mach 3 Minimum System Requirements are: CPU - Intel processor with 32-bit or 64-bit support, 1 GHz or faster processor; RAM - 1 GB; OS - Windows 2000, Windows XP, or Windows 7. A TIG 250P welding machine (2) for (GTAW) gas tungsten arc welding offering DC welding was used as a source of the plasma arc, its parameters are provided in table 2.

Table 2. Parameters of the 250P apparatus

Manufacturer	Weldcom
Type	Inverter Welders
Input Voltage (V)	220
Input Power (KVA)	6
Output Current (A)	20-180
Input Frequency (Hz)	50
Dimension(mm)	425 x 205 x 355
Duty Cycle (%)	60
Weight (Kg)	20

The frame (3) was made of an aluminum extrusion alloy. Due to the reinforced structure, it can withstand heavy loads, while maintaining reliability as well as rigidity. The movement of the torch (4) along the Ox Oz axes and tables (5, 6) along Oy are performed using ball screws, consisting of a screw of 12mm in diameter, two ball screw supports BK, nut housing GFD – 12 and nuts R12-5T4-FSI. The use of these ball screws eliminates the appearance of backlash during movement, and provides high precision processing, smoothness, and high wear resistance. The movement of the 3 jaw chuck K80 is provided by a toothed belt drive, consisting of a driving (40 teeth) and driven (20 teeth) pulleys GT2, and a belt of 10 mm width. To move the axes, stepping motors 57x42 mm with 0.8-1.8 of step angle and 3 N·m of holding torque, which allows for the use of moving parts with a weight of up to 15 kg. Tables (5,6) are used to clamp the workpiece, which is processed on the installation. The presence of a T slot in the aluminum table allows for the workpiece to be attached to any work area.

2.2 Preparation of the carburizing paste

A paste consisting of graphite, liquid glass, and water was used for carburizing [9-11]. The use of graphite as the main saturating component was due to its high electrical conductivity, which allows the reduction of electrical resistance at the contact interface between the heating spot of the plasma arc and the coating. The mechanical strength of the coating was achieved by the use of liquid glass as a binder. Based on the experiments, it was shown that a solution consisting of 33% liquid glass, 30% graphite, and 37% water gave the best result regarding the adhesion of the graphite paste (before drying) to the surface of the cylindrical samples. A further increase in the volume of liquid glass limited the diffusion of carbon atoms into the surface layers of the metal. Fig. 2 shows the process of making the graphite powder and the plasma treatment for a cylindrical sample.

After mixing, the solution was stirred with a heating magnetic stirrer for 15 minutes to form a colloidal suspension. Samples were immersed

in this solution, held for 5 seconds and rotated by 360^0 (for the cylindrical sample). Next, the samples were removed from the colloidal suspension and placed in the furnace at a temperature of 60 ^{0}C for 2 hours. Subsequently, the graphite from the solution adhered firmly to the surface of the samples and formed layers of uniform thickness. A Defelsko Positector 6000 FNS coating thickness Gauge was applied to measure the length of these layers along the sample. The coating thickness along the sample, which used 33% liquid glass, ranged from 104 to 112 µm, so there is no significant difference in coating thickness. This is explained by the fact that when using a paste, which consists of 30% graphite and 33% liquid glass, the solution viscosity is sufficient to prevent the displacement of the graphite coating layers.
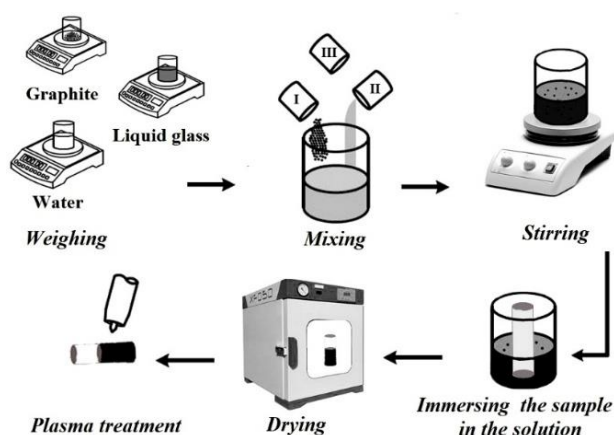
Fig. 2. The schematic diagram of a plasma carburizing process.

2.3 The carburizing process

The material used in this work was a low carbon steel St3 (Russian State Standard GOST 380-2005), which had microstructure (Fig. 3) consisting of: pearlite (dark phase) and ferrite (light phase). The composition of this steel is presented in Table 3. High-purity graphite powder EQ-Lib-CMSG was used to ensure sufficiently high electrical conductivities and enough amount of carbon for saturation process. The specification of graphite powder was indicated in Table 4. The plasma carburization was accomplished by using developed equipment and workpieces, which have a shape of cylinder (20 mm diameter and 150 mm length) and a rectangular prism (100mm length, 20 mm width and 10 mm height). Argon gas (flow rate of 5 of L/min) was used as the plasma-forming substance during the carburization process. The tungsten electrode, 2.4 mm in diameter and 150 mm in long, was kept at a distance of 2 mm from the specimen surface. The rotational speed of workpiece was set at 2800 degree/min and the plasma arc current was chosen as 90, 100, 110 and 120 A. In treatment process after cylindrical specimen made one revolution, the torch moved to the left (right) by 2 mm with speed of 10mm/s. These movements were repeated and controlled by the Mach 3 program. This ensured a highly accurate of the carburizing process.
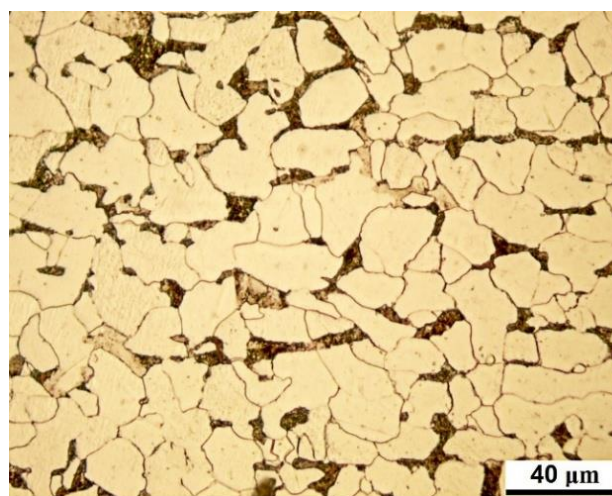

Fig. 3. The microstructure of St 3 steel before plasma treatment.

Table 3. Chemical composition of ST3 steel (GOST 380-2005).

C	Si	Mn	Ni	S	P	Cu
0.2	0.15	2	0.3	0.05	0.04	0.2

Table 4. Graphite powder specification.

Carbon (%)	Granularity (um)	Moisture (%)	Ash	Density (g/cm^3)
≥99.98	1-5	≤0.08	≤0.01	≥0.99

The microstructure was studied using an MET-2 microscope, which magnifies up to 1000 times and a scanning electron microscope JIB-4500, which provides an effective magnification of up to 22,000 times. The microhardness was measured with an HMV-2T (Shimadzu) microhardness tester under load of 2 N. The phases present in the carburization layer were identified by X-ray diffractometry (XRD) using a Shimadzu 7000 X-ray diffractometer.

3. RESULTS AND DISCUSSION

Fig. 4 depicts the current and voltage waveforms of the electric arc, which burns between the tungsten electrode and the sample, which is coated with the various graphite pastes. It can be seen that when the surface was uncoated, the electric arc burned in a stable manner (4a). The current (channel 2) and voltage (channel 1) exhibit a high degree of stability.
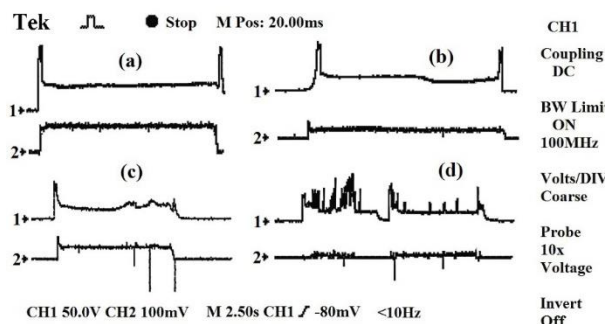

Fig. 4. Oscillogram of current and voltage when using different types of coating, (a) Without coating, (b) Liquid glass and graphite, (c) Dilute commercial graphite spray, (d) 0.1 g of carboxymethylcellulose (CMC) in 100 ml of ethanol.

The electric arcs, which burned at the metal surfaces coated with dilute commercial graphite spray [12] and 0.1 g of carboxymethylcellulose (CMC) in ethanol (100 ml) are shown in Fig 4 c, d. The treatment process was unstable because the arc discharge did not exist continuously at the specified voltage and current values. The arc current and voltage changed more drastically and erratically because the composition of these coatings includes substances that do not conduct electricity. These processes prevented the stability of arc burning. But in these works, the electrical conductivity of the coating was not a critical parameter of the laser carburizing process. This is because, when using a laser as a heat source, the electric current does not pass through the coating.

When a coating consisting of liquid glass and graphite was applied to the surface, the stability of arc burning was ensured (Fig. 4b). This is due to the fact that graphite has a high electrical conductivity, and sodium liquid glass consists of silicon oxide (SiO_2) and sodium oxide (Na_2O), which melt at high temperatures and conduct an electric current. Moreover, oxidation-reduction reactions occurred and silicon and sodium formed, which also conduct an electric current. Thus, in Fig.

4b, in the second part of the waveform, the voltage dropped due to an increase in the electrical conductivity of the coating.

After plasma arc treatment a part of the paste (upper part) remained on the sample surface, (i.e. not all the graphite was involved in the carburizing process). Liquid glass with graphite powder forms a strong layer, which protects the metal surface from melting under an optimal setting (current, voltage, speed, arc length). The study of the surface morphology showed that a thin melted layer is observed on the metal surface after processing, and consequently its roughness increases [11]. After removing the paste residue, a white layer was observed (Fig. 5, 6), on which protrusions and depressions were fixed due to microfusion (Figure 7a). A larger magnification revealed a lamellar cementite, which formed due to a direct contact of carbon from the coating with the steel (Fig. 7b).
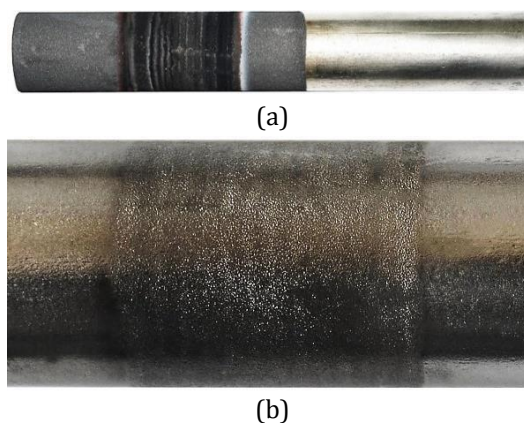

(a)

(b)

Fig. 5. Cylindrical sample after processing with multiple pass, (a) After plasma treatment, (b) After removal of the graphite coating.
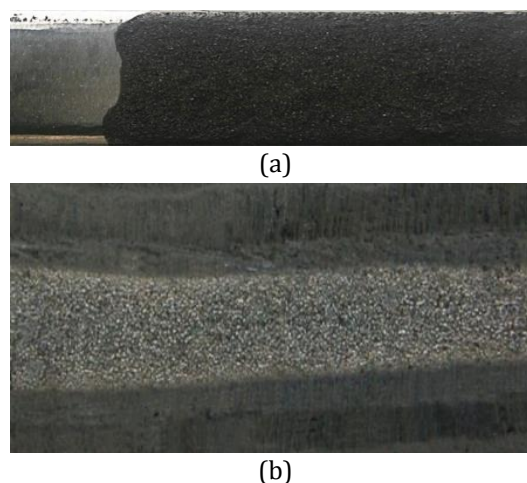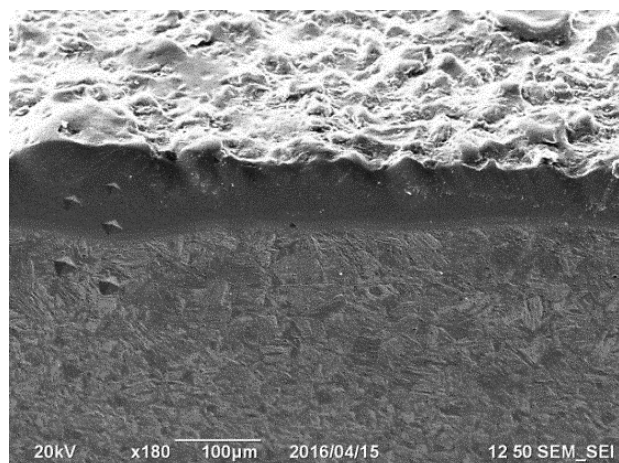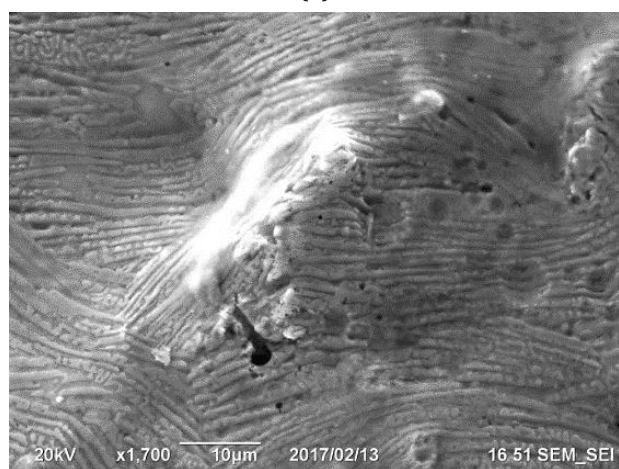

(a)

(b)

Fig. 6. Flat sample after processing with single pass (I=100A), (a) The sample with graphite paste, (b) The sample after plasma treatment.

(a)

(b)

Fig. 7. The surfaces after plasma carburization, (a) x180, (b) x1700.

A cross-section of the plasma treated specimen shown in Fig. 8 depicts the surface hardened layer, which consists of the carburized layer (CL), heat-affected zone (HAZ) and the base metal (BM). After etching in the Nital reagent, the carburized layers have a 'bright' appearance under an optical microscope [13]. As can be clearly seen in Fig. 8, the thickness of the cemented layer reaches a maximal value at the middle of the hardened track and gradually decreases to the edge due to the uneven distribution of heat in the electric arc [14].

Fig. 8. Transverse section of a laser-treated specimen (I=120 A).

The experimental data revealed that, when the current increased above 90 A, the saturation process began, then the carburized thickness increased with increasing current. Upon reaching 120 A, the carburized thickness was 175 μm. A further increase in the current value led to the melting of the sample surface, and a liquid metal bath was formed. Fig. 9 shows the dependence of the CL depth on the current during the carburizing process.
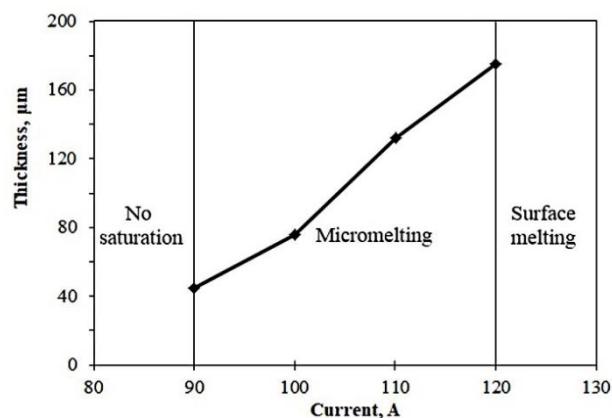

Fig. 9. Dependence of carburizing thickness on current.

The CL presents a wide variety of microstructures, which depend on the distance from the sample surface and the number of passes used. In this work, only the microstructure of the CL in the sample treated with a single pass was studied. The CLs are divided into three zones with different levels of thickness and carbon content. The first zone (upper part), whose thickness ranges from 30 to 60 μm consists of a proeutectic cementite in an eutectic matrix with a microhardness up to 1000 $HV_{0.2}$, whereas microhardness of base metal is only 200 $HV_{0.2}$. The microstructure taken by an SEM of the eutectic structure processed is shown with more detail in Fig. 10, 11 a, b. Below this zone, a mixture of the plate martensite and a retained austenite hardened by uniformly distributed cementite was observed (Fig. 11c). The amount of this decreases with increasing distance from the surface, causing a wide range of measured microharness values (500 $HV_{0.2}$ - 700 $HV_{0.2}$). The thickness of this zone reaches 70 μm and decreases from the center to the edge. The region at the bottom of the CL (the third zone or diffusion zone), having a thickness range of 10 to 30 μm consists of lath martensite (Fig. 11d) with a microhardness up to 800 $HV_{0.2}$.
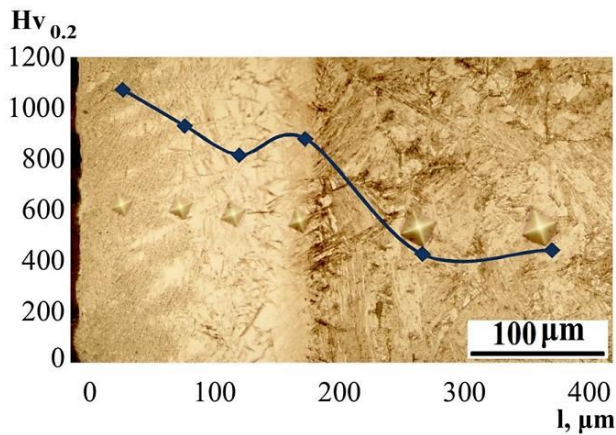
Fig. 10. Transverse section of the carburizing sample Carburized layer (C.L) and the heat –affected zone (H.A.Z).

The surface roughness after plasma cementation was studied in [11] using Form Talysurf i200 inductive systems and optical profilometer Bruker Contour GT-K1 for 3D surface measurement. Before plasma carburizing process, the metal sample was subjected to grinding to remove the oxide film. The surface roughness values (Ra) after grinding ranged from 0.7 μm to 0.9 μm (Fig. 12a). The study of the surface relief showed that a thin melted layer was observed. Depressions and protrusions were formed on the surface sample, where cementite plates and blocks were placed. Therefore, the surface roughness (Ra) increased and ranged between 1 μm and 5 μm (Fig. 12b). In addition, traces of partial melting and remnants of the coating not destroyed by the plasma arc were also observed on the surface (Fig. 12c).
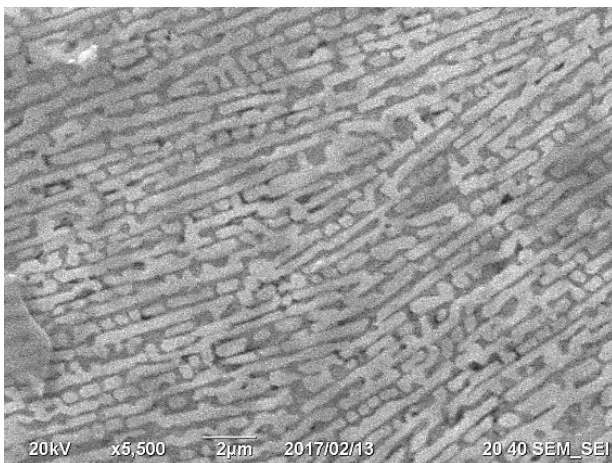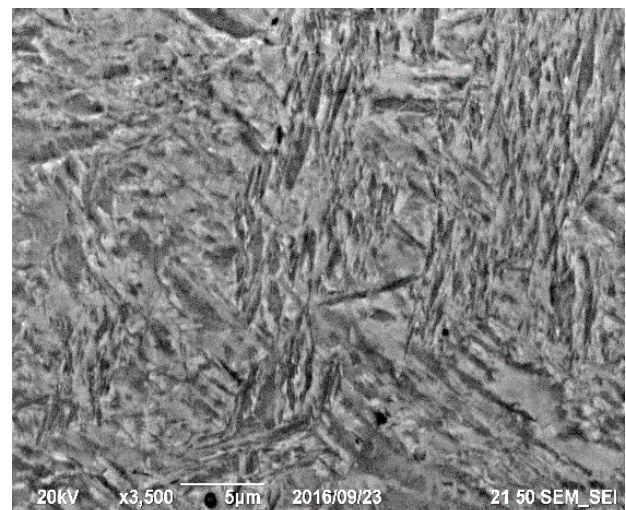

(a)
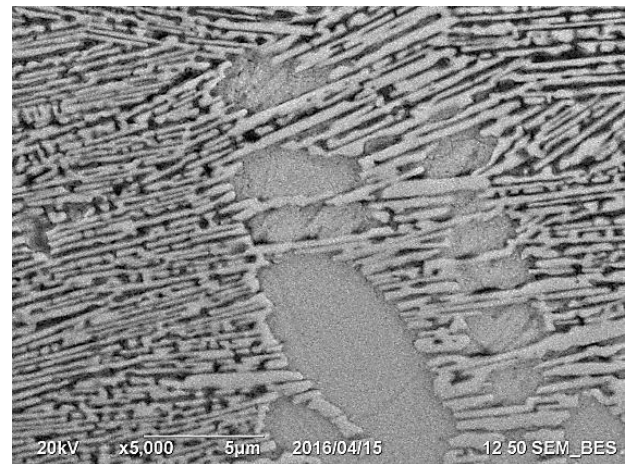
(b)
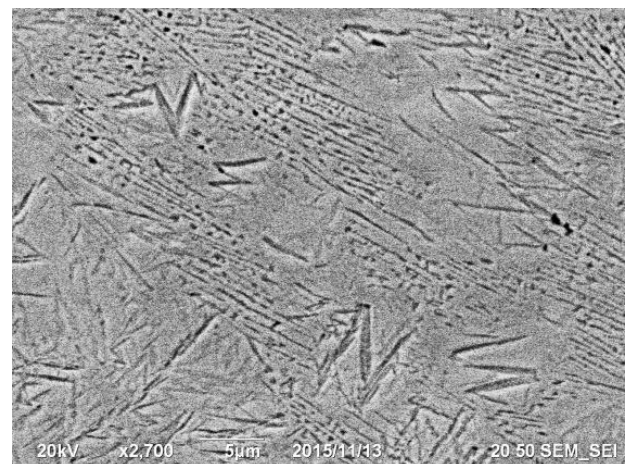
(c)

(d)

Fig. 11. Microstructure of the carburized layer, (a) Lamellar iron carbide, (b,c) Lamellar iron carbide + retained austenite + martensite, (d) Martensite.
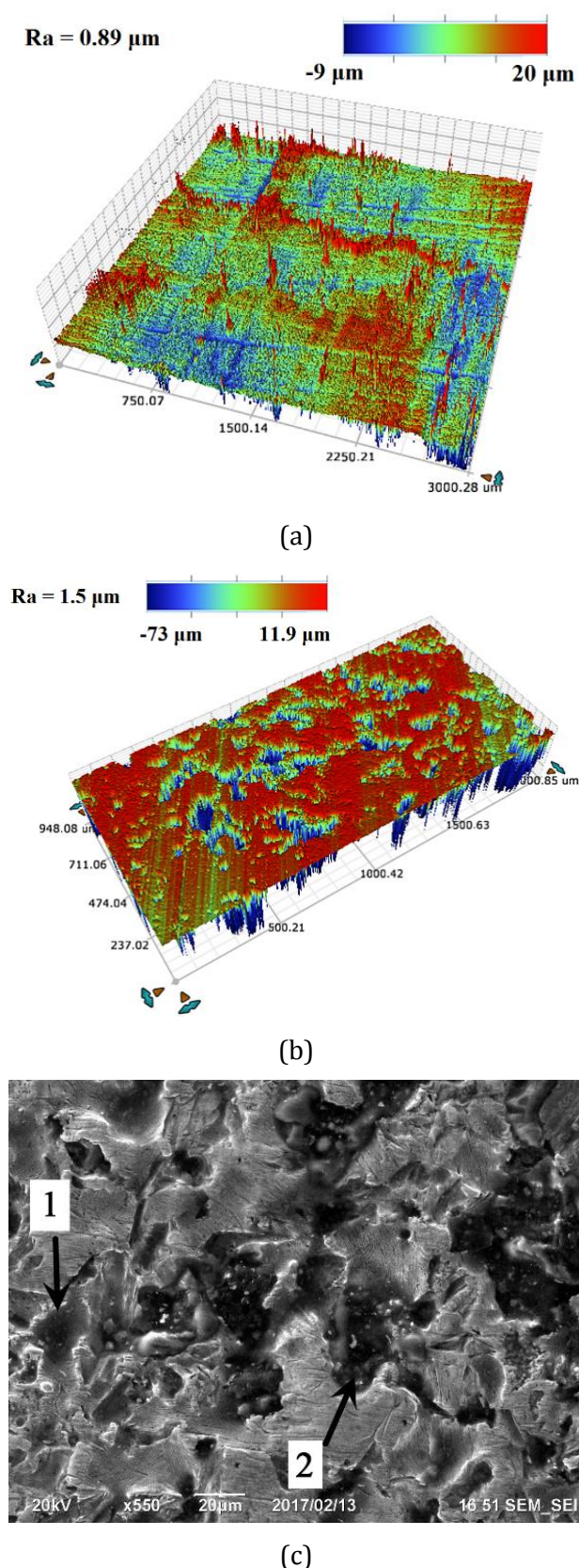
217

(a)

(b)

(c)

Fig. 12. 3D surface of flat sample, (a) After grinding, (b) After plasma carburizing with single pass, (c) Carburized surface, 1 Trace of partial melting, 2 Coating remnant.

In the crystallization process the nucleation and growth of eutectic cells is the main factor, which establishes the morphology and properties of white iron. There are two type of eutectic structure: honeycomb ledeburite and plate cementite [15,16]. In the case of honeycomb ledeburite formation once Fe_3C, leading phase, nucleates, edgewise growth of Fe_3C plate occurs rapidly (Fig. 13a). Then, during a second eutectic phase, the austenite appears on the initial base crystal, forming a rod structure perpendicular to and between the Fe_3C plates. However, the edgewise growth is more rapid than the sidewise and dominates the structure. Thus, after etching only the cross sections of the austenite rods, which assume the shape of dark round spots are observed on a white cementite plate [17]. In this work: cementite, as thin plates, alternatively distributed in the intervals of primary dendrites, and eutectic austenite often grows on primary austenite. It is therefore difficult to distinguish them from each other (Fig. 13 b). Rod-like branches are not observed on the side, and the cementite grows mainly edgewise. [18]. This type of structure is similar to plate-like cementite eutectic. A vast collection of works devoted to the mechanical properties of white iron have shown that white iron featuring a plate-like cementite eutectic manifests a better strength than a white iron with a honeycomb cementite eutectic [19]. This is because the austenite in a plate-like cementite eutectic is connected whereas the cementite features a non-continuous, isolated distribution. However, an eutectic structure with a honeycomb cementite manifests better feeding properties that ensure it is not prone to produce shrinkage-induced cracking [20]. Although the exact reasons for the formation of a plate-like cementite is not yet totally clear, it was recognized that their formation is related to melt undercooling and composition [15]

The work [7] presented investigation results of wear resistance of steel surfaces at abrasive wear after plasma carburization for different types of surface layer structures. The experimental layout was based on GOST (State Standard) 17367–71. The wear resistance of the materials was determined by measuring the reduction of the height and mass loss of the samples and the relative wear resistance was calculated using the formula (1):

$$\varepsilon = \frac{\Delta m_r}{\Delta m_t} \qquad (1)$$

where Δm_r and Δm_t are the mass losses of the reference and tested samples, g.
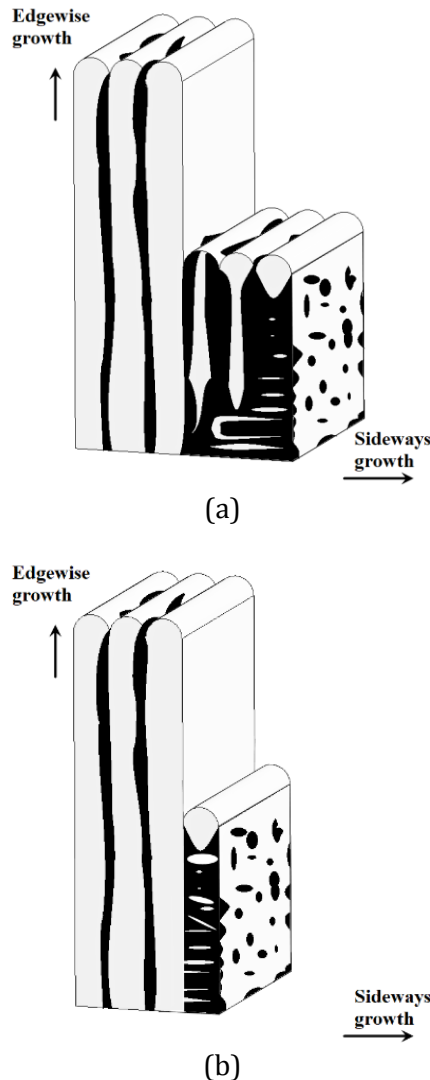

(a)

(b)

Fig. 13. Formation process of honeycomb and plate-like cementite eutectic, (a) Honeycomb eutectic, (b) Plate-like cementite eutectic.

The experimental results has shown that in conditions of interactions with fixed abrasive particles, the plasma-carburized metal surface with the eutectic structure displays an increased wear resistance up to 1.5 times in comparison to the samples carburized by a traditional furnace process. High wear resistance of the sample with eutectic structure is explained by original hardness and strong inclination toward friction-induced work hardening. This is, probably, because of a more intense dissociation (dissolving) of the defective cementite during plastic deformation under friction. The transfer of carbon atoms from cementite into the solid solution facilitates in this case blocking of dislocations found in the initial structure as well as the ones formed under frictional loading.

The formation of such a microstructure in this sample indicates a substantial increase in carbon concentration, which in turn decreases with increasing distance from the surface. XRD patterns taken at different depths of the carburizing layer are shown in Fig 14. Results of the XRD analysis indicate that the main phases of the carburization layer consist of Fe_3C, γ-Fe and α-Fe, which were observed in the optical microscopy images (Fig. 11). The peaks of the cementite were weak because of a large cementite plate and short time of plasma treatment.
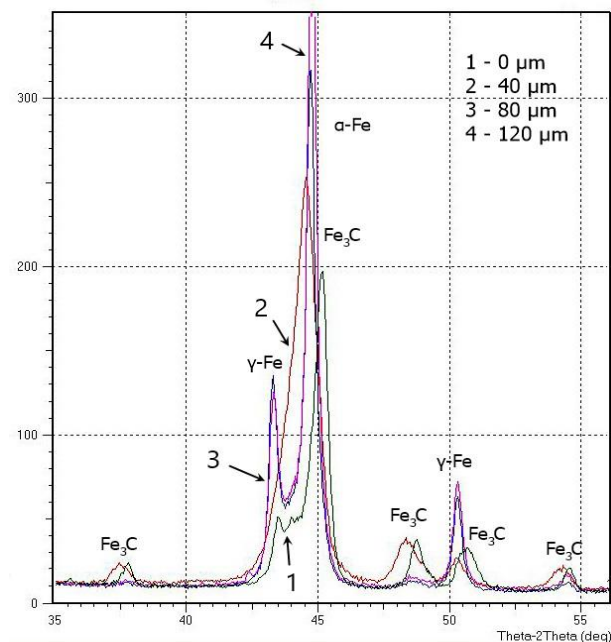

Fig. 14. XRD patterns for plasma carburized layer at different depth (I=120 A).

This is in good agreement with previously published results [13]. The amount of cementite, (55%), reached maximal value in the first zone and gradually decreased with increasing distance from the surface. This lead to a change in microhardness along the depth of carburized layer. The content of the residual austenite varied extremely and reached a maximal value of 64,24% (Fig. 15), at the depth of 120-140 μm, where mixture of austenite, martensite, cementite was obtained.
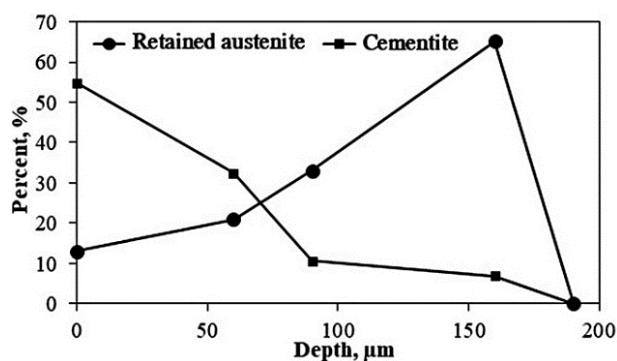
Fig. 15. The distribution of retained austenite and cementite along the depth of the cemented layer (I=120 A).

According to [21,22], the presence of a retained austenite promotes stress relaxation, which limits the process of damage accumulation and destruction of the surface layers under the action of variable impact loads. Thus, an optimal amount of austenite can reduce the risk of brittle fracture and increase the impact strength and fracture toughness of steel. It should be noted that the retained austenite, a soft phase, causing decreasing wear resistance of carburized layer only appeared in inner layers (the second and third zones) with a mixture of martensite and carbide. Therefore, the wear resistance of the carburized layer was not reduced.

4. CONCLUSIONS

The developed equipment allows automating the plasma carburizing process with high accuracy. Therefore, it is possible to significantly reduce the process time and ensure uniform quality of the saturated layer. The new type of graphite paste can be used to saturate steel with carbon using TIG welding machines, which are simple, popular and much cheaper than lasers, electronic devices or devices with a plasma jet.

The carburizing process can be achieved by two different mechanisms: a surface alloying, which involves the melting of a surface and solid state diffusion of carbon in austenite. In this case after carburizing the surface can have traces of micro-melting without metal bath formation in the form of a thin layer. Cementation depth is in the range of 30-175 μm.

Using graphite paste consisting of 30% graphite, 33% liquid glass and 37 % water allows the

formation of a hardened layer with a microhardness of 500 - 1000 $HV_{0.2}$ and yields a variety of surface microstructures, such as proeutectic cementite, retained austenite and martensite.

Acknowledgement

REFERENCES

[1] I. Koretsky, *Cementation of steel*, Leningrad, 1962.

[2] M. Kulka, A. Pertek, *Laser surface modification of carburized and borocarburized 15CrNi6 steel*, Materials Characterization, vol. 58, iss. 5, pp. 461-470, 2007, doi: 10.1016/j.matchar.2006.06.010

[3] C.J. Scheuer, R.P. Cardoso, M. Mafra, S.F. Brunatto, *AISI 420 martensitic stainless steel low-temperature plasma assisted carburizing kinetics*, Surface and Coatings Technology, vol. 214, pp. 30-37, 2013, doi: 10.1016/j.surfcoat.2012.10.060

[4] D. Santos, G. Vasconcelos, A.J. Abdalla, M.S.F. Lima, F. Souza Neto, *Surface characterization in a 300m bainitic steel laser carburizing*, Procedia Engineering, vol. 114, pp. 322-329, 2015, doi: 10.1016/j.proeng.2015.08.075

[5] A.E. Balanovskii, *Plasma surface hardening of metals*, Irkutsk: ISTU, 2006.

[6] A.E. Balanovskii, V.V. Huy, *Plasma surface carburizing with graphite paste,* Letters on materials, vol. 7, iss. 2, pp. 175-179, 2017, doi: 10.22226/2410-3535-2017-2-175-179

[7] A.E. Balanovskii, V.V. Huy, *Estimation of wear resistance of plasma-carburized steel surface in conditions of abrasive wear,* Journal of Friction and Wear, vol. 39, iss. 4, pp. 311-318, 2018, doi: 10.3103/S1068366618040025

[8] K.K. Khrenov, G.V. Vasiliev, *Arc surface hardening*, Autogenous business, vol. 10, pp. 1-5, 1950.

[9] I.D. Kulagin, A.V. Nikolaev, *Plasma jet as a source of heat in metal processing*, Welding Production, vol. 9, pp. 1-4, 1959.

[10] D.A. Dudko, S.P. Lapisa, *New possibilities of welding with a high-temperature arc compressed by a gas stream*, Automatic welding, vol. 11, pp. 39-48, 1960.

[11] V.V. Huy, *Carburizing of low-carbon steels using plasma heating of graphite coatings and technological gaseous environment*, PhD thesis, Komsomolsk on Amur State Technical University, Komsomolsk on Amur, Russia, 2018.

[12] A.I. Katsamas, G.N. Haidemenopoulos, *Laser-beam carburizing of low-alloy steels*, Surface and Coatings Technology, vol. 139, iss. 2–3, pp. 183-191, 2001, doi: 10.1016/S0257-8972(00)01061-6

[13] I.A. Bataev, M.G. Golkovskii, A.A. Losinskaya, A.A. Bataev, A.I. Popelyukh, T. Hassel, D.D. Golovin, *Non-vacuum electron-beam carburizing and surface hardening of mild steel*, Applied Surface Science, vol. 322, pp. 6-14, 2014, doi: 10.1016/j.apsusc.2014.09.137

[14] P.R.F. Teixeira, D.B. Araújo, L.A.B. Cunha, *Study of the gaussian distribution heat source model applied to numerical thermal simulations of TIG welding processes*, Science and Engineering Journal, vol. 23, iss. 1, pp. 115-122, 2014.

[15] J. Rickard, I.C. Hughes, *Eutectic Structure in White Cast Iron*, BCIRA Journal, vol. 9, pp. 11-25, 1961.

[16] Z. Jiyang, *Colour Metallography of Cast Iron - White Cast Iron (II),* China Foundry, vol. 8, no. 4, pp. 447-462, 2011.

[17] M. Trepczyńska-Łent, E. Olejnik, *Solidification front of oriented ledeburite*, Archives of foundry engineering, vol. 16, iss. 1, pp. 124-130, 2016, doi: 10.1515/afe-2016-0015

[18] R. Elliott, *Cast Iron Technology*, Butterworth - Heinemann, 1988.

[19] A. Mazur, M.M. Gasik, V.I. Mazur, *Thermal analysis of eutectic reactions of white cast irons*. Scandinavian Journal of Metallurgy, vol. 34, iss. 4, pp. 245-249, 2005, doi: 10.1111/j.1600-0692.2005.00730.x

[20] R.W. Heine, J.E. Barton, *Eutectic Solidification of White iron and its Effects on Malleable Iron Castings*, AFS Transactions, vol. 85, pp. 379-388, 1977.

[21] G. Parrish, *Carburizing: Microstructures and Properties*, ASM International, 1999.

[22] V.Y. Dorofeyev, A.N. Sviridova, Y.M. Berezhnoy, E.N. Bessarabov, K.S. Kochkarova, V.G. Tamadaev, *Rolling contact fatigue of hot-deformed powder steels with calcium microadditives*, IOP Conference Series: Materials Science and Engineering, vol. 537, iss. 2, pp. 1-7, 2019, doi: 10.1088/1757-899X/537/2/022046